

Nonclassical effects of photon-phonon antibunching in a multifield driven optomechanical cavity

Joy Ghosh,^{1,*} Shailendra K. Varshney,^{1,2} and Kapil Debnath^{2,3,†}

¹*School of Nanoscience and Technology, IIT Kharagpur, West Bengal, 721302, India*

²*Electronics and Electrical Communication Engineering Department, IIT Kharagpur, West Bengal, 721302, India*

³*School of Natural and Computing Sciences, University of Aberdeen, Aberdeen AB24 3UE, UK*

(Dated: May 7, 2024)

The nonclassical signature of a photon-phonon pair can be tested effectively by violating Cauchy-Schwarz and Bell's inequality, which can arise due to antibunching phenomena in coupled bosonic systems. In this paper, we analyze the measurement criteria imposed on the second-order coherence functions and investigate the quantum correlations leading to the suppression of multi-photon-phonon excitation in a single optomechanical cavity upon driving it with two pumping fields. It is also shown that the Cauchy-Schwarz violation can serve as an ideal precursor to demonstrate stronger tests of locality related to Bell's inequality. We consider weak driving and optomechanical coupling coefficient parameters in the system that enables the unconventional nature of photon (phonon) blockades while operating in the resonance of cavity detuning and mechanical frequency. These findings are valuable for generating sub-Poissonian signals in optimal conditions and have potential applications in hybrid systems for on-demand single photon (phonon) detection.

I. INTRODUCTION

In what sense does the quantum behavior of a pulse of light become predominant was the central question that kept the optics community busy from the middle of the 20th century. Later, the issue was resolved by the pioneering works of Glauber, Sudarshan, Mandel, and others, where the coherence functions of quantized electromagnetic fields are introduced to characterize different nonclassical effects such as antibunching, squeezing, and non-locality [1]. In this context, the most well-demonstrated examples include twin-beam generation [2], four-wave mixing [3], parametric down-conversion [4], resonance fluorescence [5], etc. The central argument for the proposal of nonclassical demonstration is the phenomena of anticorrelation in antibunching [6], which can be easily measured by implementing a ubiquitous relation in mathematical physics and engineering called the Cauchy-Schwarz (CS) inequality [7]. The CS inequality provides a classical upper bound, which states that products of two arbitrary fluctuating vectors are bounded by the squared expectation value of their cross-correlations i.e. $|\langle AB \rangle| \leq \sqrt{\langle A^2 \rangle \langle B^2 \rangle}$, where A and B are two random variable observables and any two classical signals always obey this fundamental relation. However, the antibunching property of light can violate this inequality, which is not accountable in classical optics [8]. Previously, the violation has been reported in a plethora of optical systems and atomic ensembles [9–13], as well as with matter-waves [6] and recently in magnon pairs [14]. The CS violation is also considered a major prediction of the spontaneous Hawking radiation in sonic black holes [15]. The implication of CS violation is two-fold, firstly, it

depicts the stronger quantum correlations between multimode bosonic systems which is absent in the classical picture, and secondly, it implies the possibility of non-local effects encountered in the Clauser-Horne-Shimony-Holt (CHSH) framework [6, 8]. The CHSH inequality [16] is a particular type of Bell inequality [17] that falsified the idea of local realism advocated by Einstein, Podolsky, and Rosen (EPR) in the hidden variable model [18]. Over the past decades CHSH violation has been reported on different platforms (optical, condensed matter, etc.) [19–22] which involve correlations between measurements on entangled particles that are usually represented by Bell states. Violations of the CHSH inequality have utmost importance in the current discourse of physical theories, providing evidence for the non-local phenomenon encountered in quantum systems. On a fundamental level, it is noteworthy to analyze CS and CHSH violations altogether in micro and nanomechanical systems for future quantum information and communication technologies.

Over the past decade, considerable efforts have been devoted to exploring the nonlinear interaction of nanoscale mechanical oscillators with optical cavities via radiation pressure force of light, which gave birth to the field of optomechanics (OM) [23]. Ground state cooling [24], normal mode splitting [25], entanglement between mirror and light [26], and squeezing of mechanical oscillators [27] showed breakthroughs, which brings OM a considerable participant while investigating the nonlinear quantum regime on a mesoscopic scale [28]. Thus, antibunching properties primarily featured with photons are now associated with phononic modes also [29]. In the demonstration of antibunching, a weak Kerr-like nonlinearity (alternatively known as the unconventional blockades [30]) is essential for the resonant excitation of single quanta, for this, several improvements of photon and phonon blockades in OM platforms are proposed via two-level systems [31], parametric amplification [32], spinning resonator [33], \mathcal{PT} symmetric effects [34], quadratic cou-

* joyghos@kgpian.iitkgp.ac.in

† kapil.debnath@abdn.ac.uk

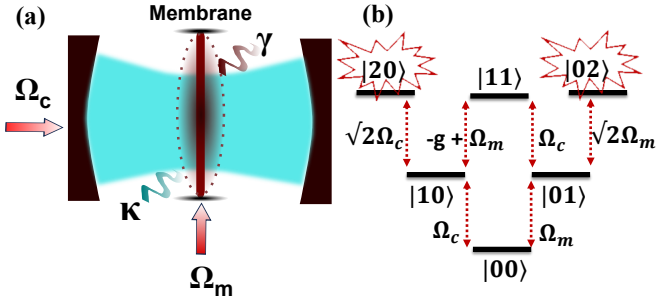


FIG. 1. (a) Schematic of a single cavity optomechanical system consisting of a membrane in the middle architecture, under two weak driving fields. The amplitude of the optical and mechanical driving fields are Ω_c and Ω_m with corresponding damping rates κ and γ . (b) Transition pathways of multiple Fock states leading destructive interference, which is responsible for the two-photon-phonon blockade.

pling [35, 36], etc. However, OM coupling itself resembles a Kerr-like effect [37], which can cause a violation of classical inequalities in a single photon-phonon-generated Fock state. On a general ground, it is possible to exhibit the CHSH violation along with the CS inequality violation in a single setup while addressing the effects of the antibunching property.

In this paper, we report a complete theoretical analysis of the CS/CHSH violation based on the strong nonclassical signature of the OM cavity, where the system is driven by two weak pump fields. For this, the second-order coherence function designed for the quantum operators is implemented to test the antibunching phenomena of optical and mechanical modes simultaneously. From analytical derivations, a single photon-phonon Fock state is established via the multiple pathway destructive interference [38], which can be generated upon resonant driving of the system, reflecting the CS/CHSH violation to a great extent. The sub-Poissonian statistics of the photon-phonon field are extracted from the joint Fock-space distribution, which holds fundamental importance in quantum optics studies. Furthermore, the single particle occupancy probability has achieved maximum in this system while operating in resonance conditions. This indicates efficient antibunching phenomena certified for the benefits of sensing and quantum control at a few photon-phonon levels.

II. THEORETICAL FRAMEWORK

Consider a standard Fabry-Pérot system, consisting of a laser-driven cavity, which causes coherent vibrations in the movable membrane as shown in Fig.1(a). The cavity frequency is assumed to be linearly coupled to the displacement of the membrane via the radiation pressure force of light. In addition to the optical driving force, an extra weak pumping is provided to excite phonons in the mechanical mode. The weak pumping field can

be implemented by using the piezoelectric effect or a dc voltage signal [39]. The Hamiltonian of this system in the rotating frame of driving frequency can be expressed as (taking $\hbar = 1$)

$$\mathcal{H} = \Delta \hat{a}^\dagger \hat{a} + \omega_m \hat{b}^\dagger \hat{b} - g \hat{a}^\dagger \hat{a} (\hat{b} + \hat{b}^\dagger) + \Omega_c \hat{a}^\dagger + \Omega_m \hat{b}^\dagger + \text{h.c.} \quad (1)$$

Here, $\Delta = \omega_c - \omega_L$ is the detuning between cavity frequency (ω_c) and driving laser frequency (ω_L), \hat{a}^\dagger (\hat{a}) are the creation (annihilation) operators associated with the optical field. The mechanical mode frequency is denoted by ω_m with respective operators \hat{b}^\dagger (\hat{b}) and g represents the optomechanical coupling strength. The amplitude of the weak mechanical pump (and laser drive) is expressed as Ω_m (Ω_c). The free part of the Hamiltonian (without driving fields) in Eq.(1) has eigenvalues of the form $E_{nm} = \Delta n + \omega_m m - g^2 n^2 / \omega_m$ (where n and m are positive integers), which showcases the anharmonicity of the energy spectrum in the cavity-membrane oscillator system. By taking the cavity (κ) and mechanical dissipation (γ) rates into account, the dynamical evolution of the system can be described by the following Lindblad master equation

$$\partial_t \rho = -i[\mathcal{H}, \rho] + \kappa \mathcal{L}(\hat{a})\rho + (n_{th} + 1)\gamma \mathcal{L}(\hat{b})\rho + n_{th}\gamma \mathcal{L}(\hat{b}^\dagger)\rho \quad (2)$$

where ρ is the density matrix and $n_{th} = 1/[\exp(\frac{\hbar\omega_m}{k_B T}) - 1]$ (where k_B is the Boltzmann constant) is the thermal phonon excitation number at temperature T , and the Lindbladian is expressed as $\mathcal{L}(\hat{o}) = \hat{o}\rho\hat{o}^\dagger - \frac{1}{2}\{\hat{o}^\dagger\hat{o}, \rho\}$; $o = \hat{a}, \hat{b}$ with $\{\cdot\}$ is the anticommutation operation. From Eq.(2), the time-delayed second-order coherence function for photons can be computed as, $g^2(\tau) = \text{Tr}[\hat{a}^\dagger \hat{a}^\dagger \hat{a} \hat{a} \rho] / \text{Tr}[\hat{a}^\dagger \hat{a} \rho]^2$, while in case of phonons, operator \hat{a} is replaced by \hat{b} . The function $g^2(\tau)$ has several properties from which the statistical nature of quanta is distinguished from the classical signal, from which the following inequalities are always satisfied, (i) $g_{ii}^2(0) \geq 1$, (ii) $g_{ii}^2(\tau) \leq g_{ii}^2(0)$, and (iii) $g_{ij}^2(0) \leq \sqrt{g_{ii}^2(0)g_{jj}^2(0)}$, where $i = \hat{a}, \hat{b}$ and $i \neq j$ [40]. The first condition describes the coherent nature of classical fields and its violation indicates the sub-Poissonian statistics of photons (phonons), while the limit $g_{ii}^2(0) \rightarrow 0$ corresponds to the blockade phenomena in which only single quanta can be excited corresponding to the optical or mechanical mode. The violation of the second and third conditions displays the effect of anticorrelation in antibunching, resulting in CS inequality not satisfying. These violations can be easily measurable by the output spectrum of an OM cavity by using a Hanbury, Brown, and Twiss-type experimental setup [41, 42]. The antibunching statistics characterized by the second-order coherence function are also linked to the Fano factor, from which mechanical limit cycles can be identified and the possibility of

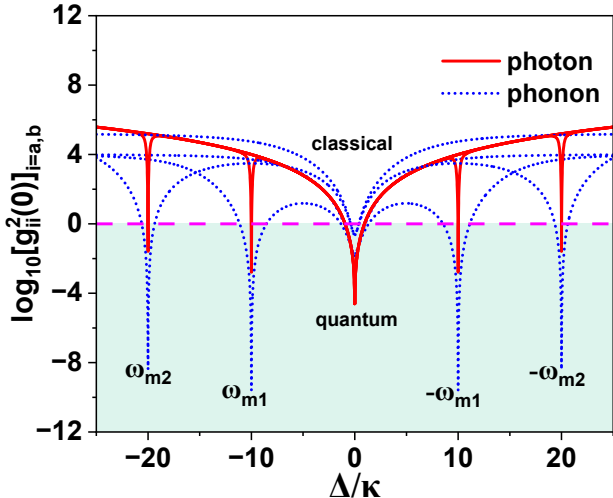


FIG. 2. Steady-state second-order coherence function $g^2(0)$ (in logarithmic scale) versus cavity detuning Δ/κ for two mechanical frequencies ($\omega_{m1} = 10\kappa$ and $\omega_{m2} = 20\kappa$) showing antibunching effect of photons (red) and phonons (blue) while operating in resonance on both sides of the central linewidth.

phonon laser is also achievable [43]. Additionally, in the case of Gaussian states, the classically forbidden values of the coherence function are observed as a consequence of optimized amplitude squeezing [44]. However, the analytical expression of the second-order coherence function $g_{ii}^2(\tau)$ is not directly solvable from the master equation Eq.(2). To better understand the physical mechanism, an alternative method is provided to breach the classical inequalities and demonstrate the antibunching phenomena in the present system. The analytical description of the temporal evolution (as well as in steady-state) of the second-order coherence function can be calculated by solving Schrödinger's equation in the truncated Fock space by assuming a weak driving condition i.e. $\{\Omega_c, \Omega_m\} \ll \{\kappa, \gamma\}$, where the possibility of multi-particle excitation can be controlled by optimizing the system parameters. Some important characterization pa-

rameters of this model are considered as, high mechanical quality factor $\omega_m/\gamma_m \gg 1$, the resolved-sideband regime $\omega_m > \kappa$, and a weak OM coupling coefficient $g < \omega_m$. Assuming the membrane has been cooled to the ground state initially ($n_{th} \approx 0$), the weak driving field can be treated as a perturbation, so the wavefunction (following the rapid communication [38]) can be expressed in the photon-phonon joint Fock space as

$$|\psi\rangle = \sum_{n,m}^{n+m \leq 2} C_{nm} |nm\rangle \quad (3)$$

where C_{nm} is the amplitude of a particular state $|n\rangle \otimes |m\rangle$ (with n photons and m phonon numbers) belonging to the wavefunction $|\psi\rangle$ with occupation probability $|C_{nm}|^2$, such that $|C_{00}| \gg |C_{10}|, |C_{01}| \gg |C_{11}|, |C_{20}|, |C_{02}|$ satisfies under weak-pumping. Considering dissipation factors of the cavity and membrane into account, the effective Hamiltonian has the following non-hermitian form written as, $\mathcal{H}_{eff} = \mathcal{H} - i\kappa/2 \hat{a}^\dagger \hat{a} - i\gamma/2 \hat{b}^\dagger \hat{b}$. Based on the Schrödinger's equation i.e. $i\partial_t |\psi\rangle = \mathcal{H}_{eff} |\psi\rangle$, the dynamical evolution of the transition probabilities C_{nm} are obtained as

$$i\partial_t C_{00} = \Omega_c C_{10} + \Omega_m C_{01} \quad (4)$$

$$i\partial_t C_{10} = \Delta' C_{10} + (-g + \Omega_m) C_{11} + \Omega_c C_{00} + \sqrt{2}\Omega_c C_{20} \quad (5)$$

$$i\partial_t C_{01} = \omega'_m C_{01} + \Omega_c C_{11} + \Omega_m C_{00} + \sqrt{2}\Omega_m C_{02} \quad (6)$$

$$i\partial_t C_{11} = (\Delta' + \omega'_m) C_{11} + (-g + \Omega_m) C_{10} + \Omega_c C_{01} \quad (7)$$

$$i\partial_t C_{20} = 2\Delta' C_{20} + \sqrt{2}\Omega_c C_{10} \quad (8)$$

$$i\partial_t C_{02} = 2\omega'_m C_{02} + \sqrt{2}\Omega_m C_{01} \quad (9)$$

with $\Delta' = \Delta - i\kappa/2$ and $\omega'_m = \omega_m - i\gamma/2$. The first equation of the probability amplitudes, i.e. Eq.(4) is always approximately satisfied, therefore we can consider $|C_{00}|^2 \approx 1$. The other transitions among the Fock states of the system can invoke photon-phonon blockade based on the quantum interference effect of multiple pathways as shown in Fig.1(b). From the steady-state analysis, the Eq.(5)-(9) is solved iteratively for C_{nm} and $g_{ii}^2(0)$ is computed as

$$g_{aa}^2(0) = \frac{\langle \hat{a}^\dagger \hat{a}^\dagger \hat{a} \hat{a} \rangle}{\langle \hat{a}^\dagger \hat{a} \rangle^2} = \frac{2|C_{20}|^2}{(|C_{10}|^2 + |C_{11}|^2 + 2|C_{20}|^2)^2} \quad (10)$$

$$g_{bb}^2(0) = \frac{\langle \hat{b}^\dagger \hat{b}^\dagger \hat{b} \hat{b} \rangle}{\langle \hat{b}^\dagger \hat{b} \rangle^2} = \frac{2|C_{02}|^2}{(|C_{01}|^2 + |C_{11}|^2 + 2|C_{02}|^2)^2} \quad (11)$$

$$g_{ab}^2(0) = \frac{\langle \hat{a}^\dagger \hat{b}^\dagger \hat{b} \hat{a} \rangle}{\langle \hat{a}^\dagger \hat{a} \rangle \langle \hat{b}^\dagger \hat{b} \rangle} = \frac{|C_{11}|^2}{(|C_{10}|^2 + |C_{11}|^2 + 2|C_{20}|^2) \times (|C_{01}|^2 + |C_{11}|^2 + 2|C_{02}|^2)} \quad (12)$$

III. RESULTS AND DISCUSSION

In this section, we determine the solutions of Eq.(10)-(12) by solving C_{nm} from Eq.(5)-(9) and depict the re-

sponse of $[g_{ii}^2(0)]_{i=a,b}$ (in logarithmic scale) as a function of normalized cavity detuning (Δ/κ) in Fig.2. For

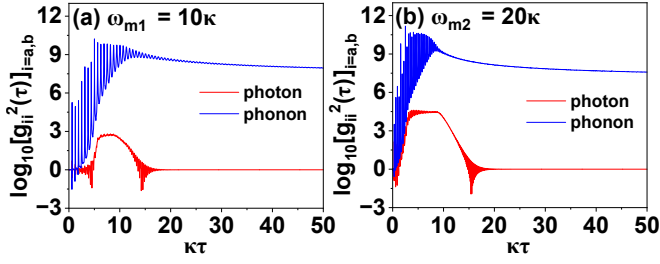


FIG. 3. Equal time-delayed second-order coherence function $\log[g^2(\tau)]$ of photons (red) and phonons (blue) versus cavity detuning Δ/κ for two mechanical frequencies $\omega_{m1} = 10\kappa$ and $\omega_{m2} = 20\kappa$, and the optomechanical coupling is set at $g = 0.25\kappa$.

the numerical simulation, the following resolved-sideband parameters are taken, the driving field strengths are chosen by considering weak pumping as $\Omega_c/\kappa = 5 \times 10^{-3}$ and $\Omega_m/\kappa = 10^{-4}$, and the mechanical damping rate is $\gamma/\kappa = 0.01$ with optomechanical coupling coefficient $g/\kappa = 0.25$. The detuning of the cavity frequency (Δ/κ) is set for a wide range and the mechanical frequency (ω_m/κ) is varied accordingly to record the response of the coherence function $g_{ii}^2(0)$ for $i = \hat{a}, \hat{b}$. From Fig.2 violation of the first inequality (proposed earlier) can be observed, showing a strong antibunching effect i.e. $\log[g_{ii}^2(0)] < 0$ for an exact condition of $\Delta = -\omega_m$. For different settings of the mechanical frequency ω_m/κ , two dips of $\log[g_{ii}^2(0)]$ are obtained respectively, first at the zeroth position of Δ and second at $\Delta = -\omega_m$. For demonstration purposes, ω_m is arbitrarily taken as 10κ and 20κ , following the good-cavity limit [45] in both blue- and red-sideband operations. The sharp response of the second-order coherence functions clearly shows that single photon-phonon blockade simultaneously exhibits in the system and the sub-Poissonian nature of the excited states is revealed only in resonance conditions. Also, by comparing the dips as $\log[g_{aa}^2(0)] \approx -2.79$ and $\log[g_{bb}^2(0)] \approx -9.58$ for $\omega_{m1} = 10\kappa$, we observe the phonon antibunching is much stronger than photons when the resonance frequency matches for both sides of the central linewidth i.e. $\Delta/\kappa > 0$ and $\Delta/\kappa < 0$. Although for the central dip, $\Delta/\kappa = 0$, the sub-Poissonian light suppresses phonon excitation with dip values noted as $\log[g_{aa}^2(0)] \approx -4.60$ and $\log[g_{bb}^2(0)] \approx -1.83$. Similar responses are also recorded for an additional resonant frequency, chosen as $\omega_{m2} = 20\kappa$. In this case, the dip values are obtained as $\log[g_{aa}^2(0)] \approx -1.59$ and $\log[g_{bb}^2(0)] \approx -8.38$, and at the central position the dip values are $\log[g_{aa}^2(0)] \approx -4.60$ and $\log[g_{bb}^2(0)] \approx -0.62$. It can be seen that the central dip of the cavity response doesn't change by shifting the mechanical frequency, however, the additional dips of the system decrease while increasing the resonant frequency to much higher values. This is because higher resonant frequencies require stronger driving strengths to maintain the quantum coherence of photons and phonons.

Next, the temporal evolution of the second-order coherence function is measured by the relation, $[g^2(\tau)_{ii}]_{i=a,b} = \langle \hat{i}^\dagger(t) \hat{i}^\dagger(t+\tau) \hat{i}(t+\tau) \hat{i}(t) \rangle / \langle \hat{i}^\dagger(t) \hat{i}(t) \rangle \langle \hat{i}^\dagger(t+\tau) \hat{i}(t+\tau) \rangle$, which depicts the joint probability of detecting one photon (phonon) at time $t = 0$ and the next emitted photon (phonon) at time $t = \tau$ [46]. The dynamics of $g_{ii}^2(\tau)$ for $i = \hat{a}, \hat{b}$ is illustrated in Fig.3, clearly showing the second inequality is also being violated i.e. $g_{ii}^2(\tau) > g_{ii}^2(0)$ exhibits for finite time delay τ . Therefore, it further reflects the sub-Poissonian statistics of the classical fields while operating on both the resonant frequencies that we have taken. Also, fluctuations of the second-order coherence function at an initial time are much lower than later instants of the transient stage, which is nothing but showcasing the antibunching effect of photons and phonons simultaneously occurring in this system.

The last and most directly applicable CS inequality proposed in the third condition reveals that the absolute square of cross-correlation of the photon and phonon fields is less than equal to the product of auto-correlations of the individual fields. To demonstrate this effect, the three functional forms of the coherence functions given in Eq.(10)-(12) are plotted by varying normalized cavity detuning (Δ/κ) and OM coupling strength (g/κ) in Fig.4. In addition, a dimensionless parameter is introduced to check the degree of classical violation, defined as $\rho = g_{ab}^2(0) / \sqrt{g_{aa}^2(0)g_{bb}^2(0)}$ [14]. Note that, $\rho > 1$ indicates the violation of CS inequality, signifying quantumness in the OM system exhibiting strong photon-phonon correlations. From Fig.4(a) and 4(b), the violation of photon-phonon coherence functions can be observed with OM coefficient variation up to the strong-coupling limit $g = 2\kappa$, while the membrane frequency is set at $\omega_m = 10\kappa$. Fig.4(c) depicts the positive cross-correlation of photon and phonon fields as a consequence of the strong antibunching effect, suggesting that the two-mode state [11], represented in Fig.1(b) is occupied. Next, the CS violation factor ρ is plotted in Fig.4(d), and we obtain $\rho \sim 9.42$, for $g = 0.25\kappa$ and $\Delta = \omega_{m1} = 10\kappa$. The lower panel of Fig.4(e)-4(h) represents similar characteristics of the coherence function obtained for the second resonance frequency at $\omega_{m2} = 20\kappa$. This demonstrates a clear shift in the cavity detuning from $\Delta/\kappa = -10$ to $\Delta/\kappa = -20$ with the violation factor found as $\rho \sim 8.79$. It can be noted that the CS violation parameter is likely to decrease with increasing the resonant frequency of the vibrating membrane.

As the CS inequality violation is established, we are set to validate the non-locality test of the antibunched photon-phonon pair generated in the OM cavity. It is expected that CHSH violation follows similar effects corresponding to the CS inequality. To confirm this, the CHSH violation factor \mathcal{B} is calculated (check the appendix for detailed calculation) and plotted in Fig.5, predicting our claim where $\mathcal{B} > 2$ is obtained again in resonance conditions only. The operating frequency of the mechanical system is set with the previous values i.e.

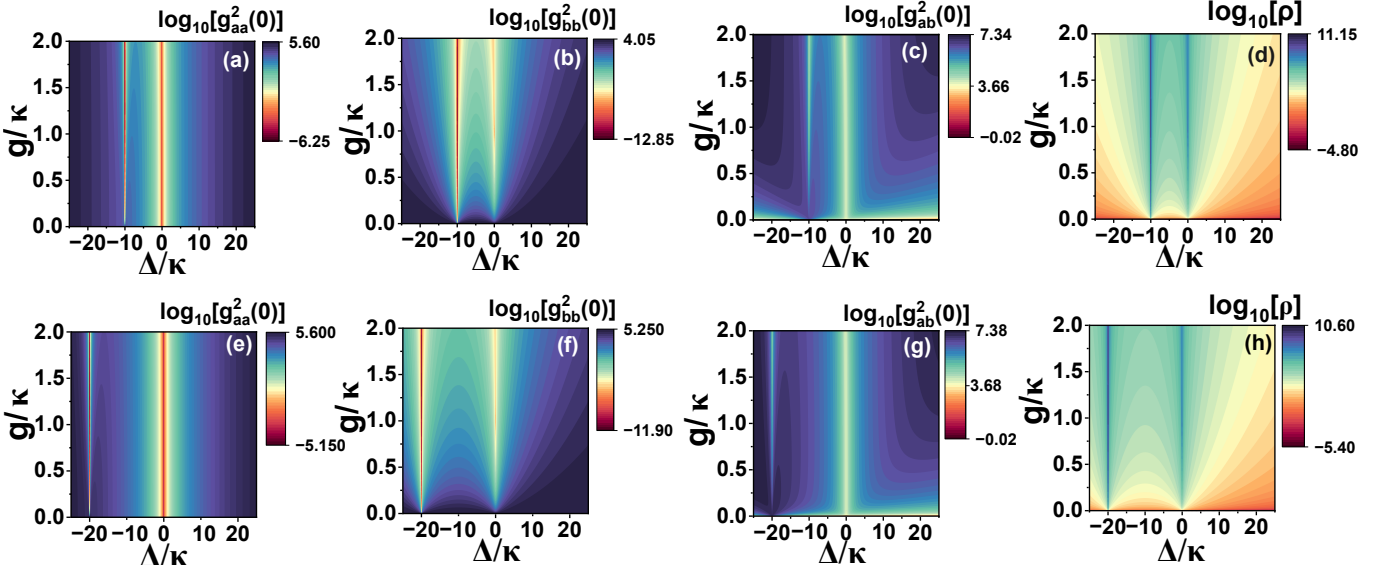


FIG. 4. Second-order coherence function $g_{ii}^2(0)$ for $i = \hat{a}, \hat{b}$ (in logarithmic scale) versus cavity detuning Δ/κ and OM coupling strength g/κ for membrane frequencies $\omega_{m1} = 10\kappa$ (upper panel) and $\omega_{m1} = 20\kappa$ (lower panel), showing the effect of anticorrelation in antibunching leading to the violation of Cauchy-Schwarz inequality.

$\omega_m = 10\kappa$ and $\omega_m = 20\kappa$ in Fig.5(a)-(b), and the CHSH violation can be visualized in a wide range of OM coefficients ranging to the strong-coupling $g = 2\kappa$. Furthermore, the maximum violation obtained is nearly equal to $2\sqrt{2}$, which is the upper limit of CHSH violation, also known as Tsirelson's bound. Lastly, a continuum of mechanical frequencies along with the cavity detuning is considered in Fig.5(c), where the CHSH violation can be realized for the whole range of resonance frequencies guaranteeing the genuine quantum nature of the photon-phonon pair in this system. Now that the CS/CHSH inequality violation is established, our claim of anticorrelation in antibunching is properly tested revealing the strong nonclassical character of optomechanical systems under optimized conditions.

To explain the earlier results more intuitively, the photon-phonon number distributions are calculated to illustrate the nonclassical properties of the second-order coherence functions. In Fig.6(a)-6(b), the steady-state mean photon (phonon) numbers i.e. $\langle \hat{a}^\dagger \hat{a} \rangle$ ($\langle \hat{b}^\dagger \hat{b} \rangle$) are plotted as a function of normalized cavity detuning Δ/κ for both the frequencies $\omega_m = 10\kappa$ and 20κ . The results agree well with the previous calculations performed on $g_{ii}^2(0)$, where peaks of distributions are obtained in the resonant frequencies only. It correctly predicts the clustered population of photons and phonons at the position $\Delta = -10\kappa$ and -20κ , respectively. Also, by comparing with the previous analysis of $g_{ii}^2(0)$ at zero detuning, the average phonon numbers are observed negligibly smaller than average photon numbers. Since the driving strength provided is very low in the system, the mean photon (phonon) numbers $\langle n_i \rangle \ll 1$ as expected. The classical limit breaks, when the average photon (phonon) number $\langle n_i \rangle_{i=a,b}$ becomes significantly smaller, as $[g_{ii}^2(0)] \geq$

$1 - 1/\langle n_i \rangle$, indicates $g_{ii}^2(0) < 1$ [8]. This is called the number-squeezing effect of the photon-phonon statistical mixture, which is quite visible in Fig.6(a)-6(b). The number-squeezing parameter can be introduced in this context, which is defined as, $\eta^2 = (\langle n^2 \rangle - \langle n \rangle^2)/n_{total}$. This is related to the auto- and cross-correlation formula by $\eta^2 = 1 + (g_{aa}^2 + g_{bb}^2 - 2g_{ab}^2 - \langle n_- \rangle^2)/\langle n_+ \rangle$, where $\langle n_- \rangle = \langle n_a \rangle - \langle n_b \rangle$ and $\langle n_+ \rangle = \langle n_a \rangle + \langle n_b \rangle$ [47]. The system is said to be number squeezed if $\eta^2 < 1$, which implies $g_{aa}^2 + g_{bb}^2 - 2g_{ab}^2 - \langle n_- \rangle^2 < 0$. A number-balanced state i.e. $\langle n_- \rangle = 0$ always gives symmetrical values of $g_{aa}^2 = g_{bb}^2$, therefore, the number-squeezing parameter can be directly linked to the CS violation factor, given by $\eta^2 = 1 + 2(1 - \rho)g_{aa}^2/\langle n_+ \rangle$. This shows that the number-squeezing of coherent fields ($\eta^2 < 1$) is responsible for the violation of CS inequality ($\rho > 1$), which can be treated as equivalent to photon-phonon entanglement. Although in the present scenario, the number state is not balanced ($g_{aa}^2 \neq g_{bb}^2$), therefore the direct link between CS inequality and squeezing parameter cannot be established due to the residual factor $\langle n_- \rangle^2$, but the physical mechanism of CS violation and its connection to the number squeezing can be interpreted by the following way.

Additionally, the deviations of the photon (phonon) distribution from the standard Poissonian distribution are calculated for the mean sample number, defined as $\log[\mathcal{P}_n/\mathcal{P}_n]$ [48], where $\mathcal{P}_n = e^{-\langle \hat{a}^\dagger \hat{a} \rangle} \langle \hat{a}^\dagger \hat{a} \rangle^n / n!$ is the standard Poisson statistics. In the case of phonons, the sample mean of the distribution is replaced by $\langle \hat{b}^\dagger \hat{b} \rangle$, and \mathcal{P}_n is the photon (phonon) number distribution, which can be found from the transition probabilities of Eq.(5)-(9). If $\mathcal{P}_n < \mathcal{P}_n$, we say the number distribution follows sub-Poissonian statistics otherwise it is called super-Poissonian in nature. For numerical representation, the

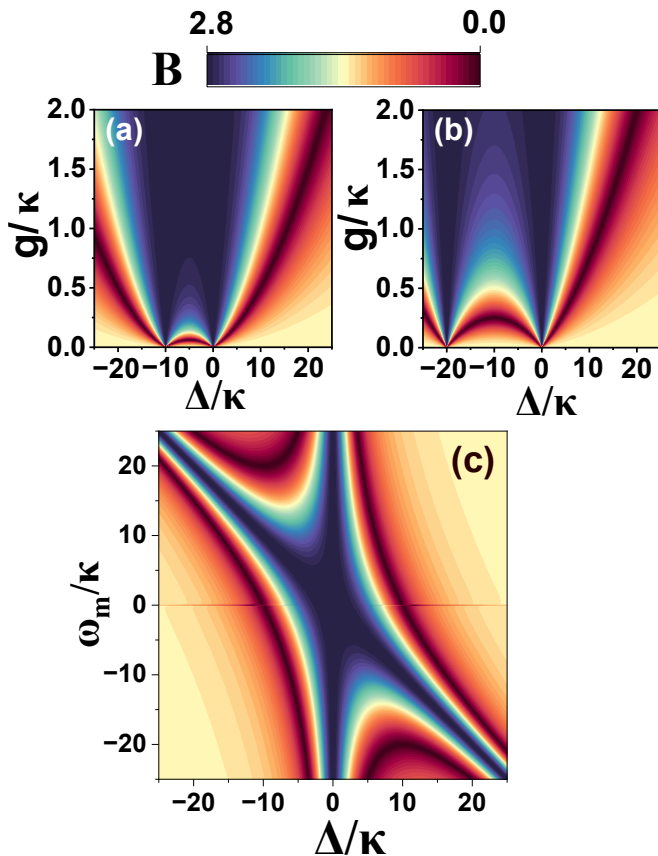


FIG. 5. Clauser-Horne-Shimony-Holt inequality violation with normalized cavity detuning and optomechanical coupling coefficient for mechanical frequencies (a) $\omega_{m1} = 10\kappa$ and (b) $\omega_{m2} = 20\kappa$. (c) CHSH violation of a continuum of mechanical frequencies with cavity detuning at fixed optomechanical coupling $g = 0.25\kappa$.

number states are truncated to three in Fig.6(c)-6(d) for both the resonant frequencies of the system and it is observed the relative population located at $\Delta = -10\kappa$ and -20κ are highly suppressed for $n \geq 2$. This confirms that the photon (phonon) tends to exist singly, revealing the sub-Poissonian statistics. Therefore it concludes our demonstration of the antibunching effect deduced from the statistics of the coherent fields incident on the OM system.

IV. EXPERIMENTAL FEASIBILITY

This section presents some remarks on the experimental prospect of the nonclassical signatures based on the photon-phonon antibunching effect in a membrane-in-the-middle optomechanical setup. The resolved-sideband parameters used in the theoretical investigation belong to the experimentally accessible parameter regimes i.e. $\omega_m > \kappa > \gamma$ [49, 50], where we tweak the optomechanical coupling strength $g < \kappa$, as the single-photon strong coupling is generally difficult to achieve. The

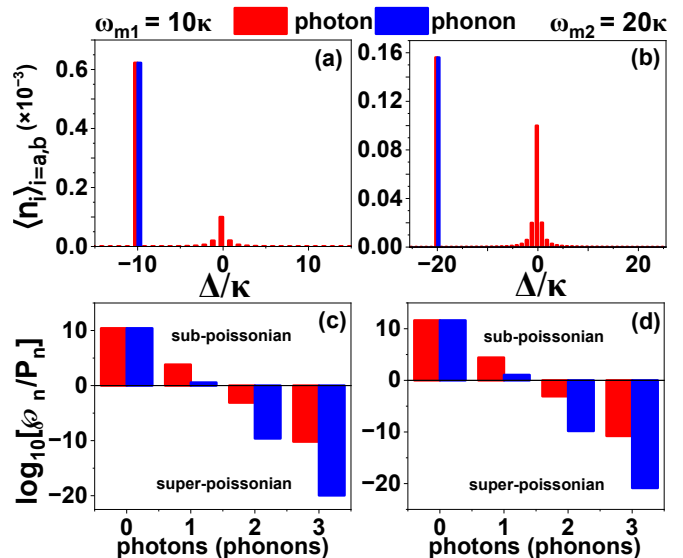


FIG. 6. (a) and (b) Photon (phonon) number distribution versus cavity detuning Δ/κ with red (blue) curves for mechanical frequencies $\omega_{m1} = 10\kappa$ and $\omega_{m2} = 20\kappa$ depicting the number squeezing effect in resonance conditions. (c) and (d) Relative deviation of the photon (phonon) distribution to the standard Poissonian distribution with the sample mean particle numbers computed at the respective resonance frequencies.

possible realization of the mechanical membrane is typically done by SiN nanoscale trampolines [51] or photonic crystal nanobeam resonators [52] having high-quality factor $\omega_m/\gamma > 10^6$ and low thermal occupation numbers $n_{th} \ll 1$ at cryogenic temperatures. For instance, the choice of parameters in our scheme is taken accordingly Ref.[53, 54], where the vibrational mode frequency of $\omega_m \approx 400$ MHz with damping rate $\gamma \approx 10^{-3}$ MHz and the cavity linewidth $\kappa \approx 0.1$ MHz is achieved. The maximum optomechanical coupling rate of $g \approx 0.05$ MHz range is observed with the ultrahigh Q toroid microcavity [55]. The detection protocol deals with the measurement of the photon-phonon sub-Poissonian field which can be done by a Hanbury-Brown-Twiss-type experiment [41, 42] for determining the second-order coherence function. Current experiments based on CS [52] and CHSH [56] violation are reported in different OM platforms, which can be combined in the current setup, satisfying all requirements of realistic parameters for the demonstration of antibunching and related nonclassical effects.

V. SUMMARY

In summary, we have investigated the antibunching effect in a multifield-driven optomechanical cavity that leads to violating Cauchy-Schwarz and CHSH inequality together. The unconventional photon (phonon) blockade effectively manifests in the current system while operating in the resonance condition between the optical cavity

detuning and the mechanical membranes' vibrating frequency. Generation of these highly nonclassical states doesn't require a single-photon-strong coupling, and the chosen parameters and techniques involved in our protocol are fully feasible under the current experimental conditions. Overall, the physical mechanism of the proposed theory largely depends on the number-squeezing of coherent fields and its connection to the classical violation of the general properties of second-order coherence functions. Moreover, these results can be generalized to a wide range of hybrid systems leading to a valid test of quantumness with currently available technology.

Appendix A: CHSH violation

In the appendix. we perform the CHSH test on the multifield-driven optomechanical cavity, which put forward the CS inequality violation as a precursor to check stronger verification of non-locality. Protocols similar to the other quantum optical systems are considered for this, where the field intensity measurement of the two modes \hat{a} and \hat{b} upon mixing with local oscillators (LO) are done in four detectors resulting in two outcomes per measurement. In the current scenario, the two modes correspond to one optical and another mechanical mode. However, the measurement of the mechanical mode is considered difficult to implement, therefore, the phononic state can be suitably mapped to a photonic state by an optomechanical parametric process [57] that converts the

antibunched photon-phonon pair into an output mode of photon-photon pair. To implement this, first, the membrane has to be cool down near the quantum ground state of motion. The OM cavity is tuned corresponding to the stoke's sideband, which generates the photon-phonon pair upon spontaneous parametric down-conversion. In this case, the interaction Hamiltonian is described by $\mathcal{H}_{int} = -G\hat{a}^\dagger\hat{b}^\dagger + \text{h.c.}$, where G is the effective OM coupling strength depends upon intracavity photon number and single-photon coupling strength g . Next, the laser detuning is changed to the red sideband to stimulate the anti-stoke process that initiates the state transfer mechanism from the phononic to the photonic mode. This mapping can be realized by the interaction Hamiltonian $\mathcal{H}_{int} = -G\hat{a}^\dagger\hat{b} + \text{h.c.}$ Now the resulting output fields that are generated from the optomechanical parametric interactions can be analyzed via photodetector intensities given by, $\langle I_{A_+} \rangle$, $\langle I_{A_-} \rangle$, $\langle I_{B_+} \rangle$, and $\langle I_{B_-} \rangle$ with adjustable polarization angles θ and ϕ of the LO. The expectations of the intensity correlations is measured followed by a beam-splitter transformation of the original modes given as

$$\begin{pmatrix} A_+ \\ A_- \end{pmatrix} = \begin{pmatrix} \cos \theta & \sin \theta \\ -\sin \theta & \cos \theta \end{pmatrix} \begin{pmatrix} a \\ b \end{pmatrix} \quad (\text{A1})$$

$$\begin{pmatrix} B_+ \\ B_- \end{pmatrix} = \begin{pmatrix} \cos \phi & -\sin \phi \\ \sin \phi & \cos \phi \end{pmatrix} \begin{pmatrix} a \\ b \end{pmatrix} \quad (\text{A2})$$

Finally, the four correlated pairs of the field intensity measurements i.e. $\langle I_{A_+} I_{B_+} \rangle$, $\langle I_{A_+} I_{B_-} \rangle$, $\langle I_{A_-} I_{B_+} \rangle$ and $\langle I_{A_-} I_{B_-} \rangle$ are done using a Mach-Zehnder interferometer and the following CHSH parameter is estimated

$$\begin{aligned} E(\theta, \phi) &= \frac{\langle I_{A_+} I_{B_+} \rangle + \langle I_{A_-} I_{B_-} \rangle - \langle I_{A_+} I_{B_-} \rangle - \langle I_{A_-} I_{B_+} \rangle}{\langle I_{A_+} I_{B_+} \rangle + \langle I_{A_-} I_{B_-} \rangle + \langle I_{A_+} I_{B_-} \rangle + \langle I_{A_-} I_{B_+} \rangle} \\ &= \frac{\langle (I_{A_+} - I_{A_-})(I_{B_+} - I_{B_-}) \rangle}{\langle (I_{A_+} + I_{A_-})(I_{B_+} + I_{B_-}) \rangle} \\ &= \frac{\langle : (A_+^\dagger A_+ - A_-^\dagger A_-)(B_+^\dagger B_+ - B_-^\dagger B_-) : \rangle}{\langle : (A_+^\dagger A_+ + A_-^\dagger A_-)(B_+^\dagger B_+ + B_-^\dagger B_-) : \rangle} \quad (\langle : \cdot : \rangle \equiv \text{normal ordering of operators}) \end{aligned} \quad (\text{A3})$$

Measurement of the first outcome is

$$\begin{aligned} A_+^\dagger A_+ + A_-^\dagger A_- &= (\hat{a}^\dagger \ \hat{b}^\dagger) \begin{pmatrix} \cos \theta & \sin \theta \\ -\sin \theta & \cos \theta \end{pmatrix} \\ &\times \begin{pmatrix} \cos \theta & \sin \theta \\ -\sin \theta & \cos \theta \end{pmatrix}^T \begin{pmatrix} \hat{a}^\dagger \\ \hat{b}^\dagger \end{pmatrix} = \hat{a}^\dagger \hat{a} + \hat{b}^\dagger \hat{b} \end{aligned}$$

Similarly, for the second measurement

$$\begin{aligned} B_+^\dagger B_+ + B_-^\dagger B_- &= (\hat{a}^\dagger \ \hat{b}^\dagger) \begin{pmatrix} \cos \phi & -\sin \phi \\ \sin \phi & \cos \phi \end{pmatrix} \\ &\times \begin{pmatrix} \cos \phi & -\sin \phi \\ \sin \phi & \cos \phi \end{pmatrix}^T \begin{pmatrix} \hat{a}^\dagger \\ \hat{b}^\dagger \end{pmatrix} = \hat{a}^\dagger \hat{a} + \hat{b}^\dagger \hat{b} \end{aligned}$$

The denominator of $E(\theta, \phi)$ is computed as

$$\begin{aligned} \langle : (A_+^\dagger A_+ + A_-^\dagger A_-)(B_+^\dagger B_+ + B_-^\dagger B_-) : \rangle &= \langle : (\hat{a}^\dagger \hat{a} + \hat{b}^\dagger \hat{b})^2 : \rangle \\ &= \langle \hat{a}^{\dagger 2} \hat{a}^2 \rangle + \langle \hat{b}^{\dagger 2} \hat{b}^2 \rangle + 2\langle \hat{a}^\dagger \hat{b}^\dagger \hat{b} \hat{a} \rangle \end{aligned}$$

For the third measurement

$$\begin{aligned} A_+^\dagger A_+ - A_-^\dagger A_- &= (\hat{a}^\dagger \ \hat{b}^\dagger) \begin{pmatrix} \cos \theta & \sin \theta \\ \sin \theta & -\cos \theta \end{pmatrix} \\ &\times \begin{pmatrix} \cos \theta & \sin \theta \\ -\sin \theta & \cos \theta \end{pmatrix} \begin{pmatrix} \hat{a}^\dagger \\ \hat{b}^\dagger \end{pmatrix} \\ &= (\hat{a}^\dagger \hat{a} - \hat{b}^\dagger \hat{b}) \cos 2\theta + (\hat{a}^\dagger \hat{b} + \hat{b}^\dagger \hat{a}) \sin 2\theta \end{aligned}$$

Finally, the last measurement is

$$\begin{aligned} B_+^\dagger B_+ - B_-^\dagger B_- &= (\hat{a}^\dagger \ \hat{b}^\dagger) \begin{pmatrix} \cos \phi & -\sin \phi \\ -\sin \phi & -\cos \phi \end{pmatrix} \\ &\times \begin{pmatrix} \cos \phi & -\sin \phi \\ \sin \phi & \cos \phi \end{pmatrix} \begin{pmatrix} \hat{a}^\dagger \\ \hat{b}^\dagger \end{pmatrix} \\ &= (\hat{a}^\dagger \hat{a} - \hat{b}^\dagger \hat{b}) \cos 2\phi - (\hat{a}^\dagger \hat{b} + \hat{b}^\dagger \hat{a}) \sin 2\phi \end{aligned}$$

The numerator of $E(\theta, \phi)$ is computed as

$$\begin{aligned} &\langle : (A_+^\dagger A_+ - A_-^\dagger A_-) (B_+^\dagger B_+ - B_-^\dagger B_-) : \rangle \\ &= \langle : [(\hat{a}^\dagger \hat{a} - \hat{b}^\dagger \hat{b}) \cos 2\theta + (\hat{a}^\dagger \hat{b} + \hat{b}^\dagger \hat{a}) \sin 2\theta] \\ &\times [(\hat{a}^\dagger \hat{a} - \hat{b}^\dagger \hat{b}) \cos 2\phi - (\hat{a}^\dagger \hat{b} + \hat{b}^\dagger \hat{a}) \sin 2\phi] : \rangle \end{aligned}$$

$$\begin{aligned} E(\theta, \phi) &= \frac{1}{\langle \hat{a}^{\dagger 2} \hat{a}^2 \rangle + \langle \hat{b}^{\dagger 2} \hat{b}^2 \rangle + 2\langle \hat{a}^\dagger \hat{b}^\dagger \hat{b} \hat{a} \rangle} \times \left[\langle (\hat{a}^\dagger \hat{a} - \hat{b}^\dagger \hat{b})^2 \rangle \cos 2\theta \cos 2\phi - \langle (\hat{a}^\dagger \hat{b} + \hat{b}^\dagger \hat{a})^2 \rangle \times \sin 2\theta \sin 2\phi \right. \\ &\quad \left. - \langle \hat{a}^\dagger \hat{a} - \hat{b}^\dagger \hat{b} \rangle \langle \hat{a}^\dagger \hat{b} + \hat{b}^\dagger \hat{a} \rangle \cos 2\theta \sin 2\phi + \langle \hat{a}^\dagger \hat{b} + \hat{b}^\dagger \hat{a} \rangle \langle \hat{a}^\dagger \hat{a} - \hat{b}^\dagger \hat{b} \rangle \sin 2\theta \cos 2\phi \right] \end{aligned} \quad (\text{A4})$$

The CHSH inequality can be tested by violating the following expression which falsifies the idea of local realism, given as

$$\mathcal{B} = |E(\theta, \phi) + E(\theta', \phi') + E(\theta', \phi) - E(\theta, \phi')| \leq 2 \quad (\text{A5})$$

with the maximum violation can be obtained by the standard choice of polarization angles chosen as $\theta = 0, \phi = \pi/8, \theta' = \pi/4, \phi' = 3\pi/8$. In terms of the original OM

Therefore, Eq.(A3) is simplified as

modes Eq.(A5) can be rewritten as

$$\mathcal{B} = \sqrt{2} \left| \frac{\langle \hat{a}^{\dagger 2} \hat{a}^2 \rangle + \langle \hat{b}^{\dagger 2} \hat{b}^2 \rangle - \langle \hat{a}^{\dagger 2} \hat{b}^2 \rangle - \langle \hat{b}^{\dagger 2} \hat{a}^2 \rangle - 4\langle \hat{a}^\dagger \hat{b}^\dagger \hat{b} \hat{a} \rangle}{\langle \hat{a}^{\dagger 2} \hat{a}^2 \rangle + \langle \hat{b}^{\dagger 2} \hat{b}^2 \rangle + 2\langle \hat{a}^\dagger \hat{b}^\dagger \hat{b} \hat{a} \rangle} \right| \quad (\text{A6})$$

It is now straightforward to calculate the CHSH violation factor \mathcal{B} by replacing the expectation values of the operators \hat{a} and \hat{b} with the transition probabilities obtained from Eq.(5)-(9). The final expression of \mathcal{B} is given by

$$\mathcal{B} = \frac{1}{\sqrt{2}} \left| \frac{2|C_{20}|^2 + 2|C_{02}|^2 - 4|C_{20}||C_{20}| - 4|C_{11}|^2}{|C_{20}|^2 + |C_{02}|^2 + |C_{11}|^2} \right| \quad (\text{A7})$$

-
- [1] G. S. Agarwal, *Quantum optics* (Cambridge University Press, 2012).
- [2] R. Bücker, J. Grond, S. Manz, T. Berrada, T. Betz, C. Koller, U. Hohenester, T. Schumm, A. Perrin, and J. Schmiedmayer, Twin-atom beams, *Nature Physics* **7**, 608 (2011).
- [3] A. M. Marino, V. Boyer, and P. D. Lett, Violation of the cauchy-schwarz inequality in the macroscopic regime, *Physical review letters* **100**, 233601 (2008).
- [4] R. Luo, H. Jiang, S. Rogers, H. Liang, Y. He, and Q. Lin, On-chip second-harmonic generation and broadband parametric down-conversion in a lithium niobate

- microresonator, *Optics express* **25**, 24531 (2017).
- [5] H. J. Kimble, M. Dagenais, and L. Mandel, Photon antibunching in resonance fluorescence, *Phys. Rev. Lett.* **39**, 691 (1977).
- [6] K. Kheruntsyan, J.-C. Jaskula, P. Deuar, M. Bonneau, G. B. Partridge, J. Ruaudel, R. Lopes, D. Boiron, and C. I. Westbrook, Violation of the cauchy-schwarz inequality with matter waves, *Physical review letters* **108**, 260401 (2012).
- [7] J. Steele, *The Cauchy-Schwarz Master Class: An Introduction to the Art of Mathematical Inequalities*, MAA problem books series (Cambridge University Press,

- 2004).
- [8] M. Reid and D. Walls, Violations of classical inequalities in quantum optics, *Physical Review A* **34**, 1260 (1986).
 - [9] N. A. Ansari and M. S. Zubairy, Violation of cauchy-schwarz and bell's inequalities in four-wave mixing, *Physical Review A* **38**, 2380 (1988).
 - [10] C. S. Muñoz, E. del Valle, C. Tejedor, and F. P. Laussy, Violation of classical inequalities by photon frequency filtering, *Physical Review A* **90**, 052111 (2014).
 - [11] H. Wu and M. Xiao, Bright correlated twin beams from an atomic ensemble in the optical cavity, *Physical Review A* **80**, 063415 (2009).
 - [12] M. Trif and P. Simon, Photon cross-correlations emitted by a josephson junction in two microwave cavities, *Physical Review B* **92**, 014503 (2015).
 - [13] M. O. Araújo, L. S. Marinho, and D. Felinto, Observation of nonclassical correlations in biphotons generated from an ensemble of pure two-level atoms, *Physical Review Letters* **128**, 083601 (2022).
 - [14] Y. Fan, J. Li, and Y. Wu, Nonclassical magnon pair generation and cauchy-schwarz inequality violation, *Physical Review A* **108**, 053715 (2023).
 - [15] J. M. de Nova, F. Sols, and I. Zapata, Violation of cauchy-schwarz inequalities by spontaneous hawking radiation in resonant boson structures, *Physical Review A* **89**, 043808 (2014).
 - [16] J. F. Clauser, M. A. Horne, A. Shimony, and R. A. Holt, Proposed experiment to test local hidden-variable theories, *Physical review letters* **23**, 880 (1969).
 - [17] J. S. Bell, *Speakable and unspeakable in quantum mechanics: Collected papers on quantum philosophy* (Cambridge university press, 2004).
 - [18] A. Einstein, B. Podolsky, and N. Rosen, Can quantum-mechanical description of physical reality be considered complete?, *Physical review* **47**, 777 (1935).
 - [19] B. Hensen, H. Bernien, A. E. Dréau, A. Reiserer, N. Kalb, M. S. Blok, J. Ruitenbergh, R. F. Vermeulen, R. N. Schouten, C. Abellán, *et al.*, Loophole-free bell inequality violation using electron spins separated by 1.3 kilometres, *Nature* **526**, 682 (2015).
 - [20] A. Palacios-Laloy, F. Mallet, F. Nguyen, P. Bertet, D. Vion, D. Esteve, and A. N. Korotkov, Experimental violation of a bell's inequality in time with weak measurement, *Nature Physics* **6**, 442 (2010).
 - [21] S. Storz, J. Schär, A. Kulikov, P. Magnard, P. Kurpiers, J. Lütolf, T. Walter, A. Copetudo, K. Reuer, A. Akin, *et al.*, Loophole-free bell inequality violation with superconducting circuits, *Nature* **617**, 265 (2023).
 - [22] M. Ansmann, H. Wang, R. C. Bialczak, M. Hofheinz, E. Lucero, M. Neeley, A. D. O'Connell, D. Sank, M. Weides, J. Wenner, *et al.*, Violation of bell's inequality in josephson phase qubits, *Nature* **461**, 504 (2009).
 - [23] M. Aspelmeyer, T. J. Kippenberg, and F. Marquardt, Cavity optomechanics, *Reviews of Modern Physics* **86**, 1391 (2014).
 - [24] J. Guo, R. Norte, and S. Gröblacher, Feedback cooling of a room temperature mechanical oscillator close to its motional ground state, *Physical review letters* **123**, 223602 (2019).
 - [25] J. M. Dobrindt, I. Wilson-Rae, and T. J. Kippenberg, Parametric normal-mode splitting in cavity optomechanics, *Physical Review Letters* **101**, 263602 (2008).
 - [26] D. Vitali, S. Gigan, A. Ferreira, H. Böhm, P. Tombesi, A. Guerreiro, V. Vedral, A. Zeilinger, and M. Aspelmeyer, Optomechanical entanglement between a movable mirror and a cavity field, *Physical review letters* **98**, 030405 (2007).
 - [27] J. Ghosh, S. Mondal, S. K. Varshney, and K. Debnath, Simultaneous control of quantum phase synchronization and entanglement dynamics in a gain-loss optomechanical cavity system, *Phys. Rev. A* **109**, 023512 (2024).
 - [28] S. Barzanjeh, A. Xuereb, S. Gröblacher, M. Paternostro, C. A. Regal, and E. M. Weig, Optomechanics for quantum technologies, *Nature Physics* **18**, 15 (2022).
 - [29] B. S. Humphries, D. Green, M. O. Borgh, and G. A. Jones, Phonon signatures in photon correlations, *Physical Review Letters* **131**, 143601 (2023).
 - [30] T. C. H. Liew and V. Savona, Single photons from coupled quantum modes, *Phys. Rev. Lett.* **104**, 183601 (2010).
 - [31] H. Wang, X. Gu, Y.-x. Liu, A. Miranowicz, and F. Nori, Tunable photon blockade in a hybrid system consisting of an optomechanical device coupled to a two-level system, *Physical Review A* **92**, 033806 (2015).
 - [32] D.-Y. Wang, C.-H. Bai, X. Han, S. Liu, S. Zhang, and H.-F. Wang, Enhanced photon blockade in an optomechanical system with parametric amplification, *Optics Letters* **45**, 2604 (2020).
 - [33] R. Huang, A. Miranowicz, J.-Q. Liao, F. Nori, and H. Jing, Nonreciprocal photon blockade, *Physical review letters* **121**, 153601 (2018).
 - [34] D.-Y. Wang, C.-H. Bai, S. Liu, S. Zhang, and H.-F. Wang, Distinguishing photon blockade in a pt-symmetric optomechanical system, *Physical Review A* **99**, 043818 (2019).
 - [35] J.-Q. Liao, F. Nori, *et al.*, Photon blockade in quadratically coupled optomechanical systems, *Physical Review A* **88**, 023853 (2013).
 - [36] H. Xie, C.-G. Liao, X. Shang, M.-Y. Ye, and X.-M. Lin, Phonon blockade in a quadratically coupled optomechanical system, *Physical Review A* **96**, 013861 (2017).
 - [37] S. Aldana, C. Bruder, and A. Nunnenkamp, Equivalence between an optomechanical system and a kerr medium, *Physical Review A* **88**, 043826 (2013).
 - [38] M. Bamba, A. Imamoglu, I. Carusotto, and C. Ciuti, Origin of strong photon antibunching in weakly nonlinear photonic molecules, *Physical Review A* **83**, 021802 (2011).
 - [39] X.-W. Xu, Y.-x. Liu, C.-P. Sun, and Y. Li, Mechanical pt symmetry in coupled optomechanical systems, *Physical Review A* **92**, 013852 (2015).
 - [40] A. Miranowicz, M. Bartkowiak, X. Wang, Y.-x. Liu, and F. Nori, Testing nonclassicality in multimode fields: A unified derivation of classical inequalities, *Physical Review A* **82**, 013824 (2010).
 - [41] R. H. Brown and R. Q. Twiss, Correlation between photons in two coherent beams of light, *Nature* **177**, 27 (1956).
 - [42] J. D. Cohen, S. M. Meenehan, G. S. MacCabe, S. Gröblacher, A. H. Safavi-Naeini, F. Marsili, M. D. Shaw, and O. Painter, Phonon counting and intensity interferometry of a nanomechanical resonator, *Nature* **520**, 522 (2015).
 - [43] N. Lörch and K. Hammerer, Sub-poissonian phonon lasing in three-mode optomechanics, *Physical Review A* **91**, 061803 (2015).
 - [44] M.-A. Lemonde, N. Didier, and A. A. Clerk, Antibunching and unconventional photon blockade with gaussian

- squeezed states, *Physical Review A* **90**, 063824 (2014).
- [45] A. Nunnenkamp, K. Børkje, and S. M. Girvin, Single-photon optomechanics, *Physical review letters* **107**, 063602 (2011).
- [46] S. Huang and G. Agarwal, Normal-mode splitting and antibunching in stokes and anti-stokes processes in cavity optomechanics: radiation-pressure-induced four-wave-mixing cavity optomechanics, *Physical Review A* **81**, 033830 (2010).
- [47] T. Wasak, P. Szańkowski, P. Ziń, M. Trippenbach, and J. Chwedeńczuk, Cauchy-schwarz inequality and particle entanglement, *Physical Review A* **90**, 033616 (2014).
- [48] C. Zhao, X. Li, S. Chao, R. Peng, C. Li, and L. Zhou, Simultaneous blockade of a photon, phonon, and magnon induced by a two-level atom, *Physical Review A* **101**, 063838 (2020).
- [49] J. Thompson, B. Zwickl, A. Jayich, F. Marquardt, S. Girvin, and J. Harris, Strong dispersive coupling of a high-finesse cavity to a micromechanical membrane, *Nature* **452**, 72 (2008).
- [50] J. C. Sankey, C. Yang, B. M. Zwickl, A. M. Jayich, and J. G. Harris, Strong and tunable nonlinear optomechanical coupling in a low-loss system, *Nature Physics* **6**, 707 (2010).
- [51] X. Wei, J. Sheng, C. Yang, Y. Wu, and H. Wu, Controllable two-membrane-in-the-middle cavity optomechanical system, *Physical Review A* **99**, 023851 (2019).
- [52] R. Riedinger, S. Hong, R. A. Norte, J. A. Slater, J. Shang, A. G. Krause, V. Anant, M. Aspelmeyer, and S. Gröblacher, Non-classical correlations between single photons and phonons from a mechanical oscillator, *Nature* **530**, 313 (2016).
- [53] H. Xie, C.-G. Liao, X. Shang, Z.-H. Chen, and X.-M. Lin, Optically induced phonon blockade in an optomechanical system with second-order nonlinearity, *Physical Review A* **98**, 023819 (2018).
- [54] T.-S. Yin, X.-Y. Lü, L.-L. Zheng, M. Wang, S. Li, and Y. Wu, Nonlinear effects in modulated quantum optomechanics, *Physical Review A* **95**, 053861 (2017).
- [55] D. Armani, T. Kippenberg, S. Spillane, and K. Vahala, Ultra-high-q toroid microcavity on a chip, *Nature* **421**, 925 (2003).
- [56] I. Marinković, A. Wallucks, R. Riedinger, S. Hong, M. Aspelmeyer, and S. Gröblacher, Optomechanical bell test, *Physical review letters* **121**, 220404 (2018).
- [57] V. C. Vivoli, T. Barnea, C. Galland, and N. Sangouard, Proposal for an optomechanical bell test, *Physical review letters* **116**, 070405 (2016).